Crack Equivalent Concept Applied to the Fracture Characterization of Bonded Joints under Pure Mode I Loading

M.F.S.F. de Moura, R.D.S.G. Campilho, J.P.M. Gonçalves

Crack Equivalent Concept Applied to the Fracture Characterization of Bonded Joints under Pure Mode I Loading

M.F.S.F. de Moura, R.D.S.G. Campilho, J.P.M. Gonçalves

PII: S0266-3538(08)00126-7
DOI: 10.1016/j.compscitech.2008.04.003
Reference: CSTE 4028

To appear in: *Composites Science and Technology*

Received Date: 30 November 2007
Revised Date: 28 March 2008
Accepted Date: 5 April 2008

Please cite this article as: de Moura, M.F.S.F., Campilho, R.D.S.G., Gonçalves, J.P.M., Crack Equivalent Concept Applied to the Fracture Characterization of Bonded Joints under Pure Mode I Loading, *Composites Science and Technology* (2008), doi: 10.1016/j.compscitech.2008.04.003

Crack Equivalent Concept Applied to the Fracture Characterization of Bonded Joints under Pure Mode I Loading

MFSF de Moura*, RDSG Campilho* and JPM Gonçalves**
* Departamento de Engenharia Mecânica e Gestão Industrial, Faculdade de Engenharia da Universidade do Porto, Rua Dr. Roberto Frias, s/n, 4200-465 Porto, Portugal
** Mathematical Sciences Department, IBM T. J. Watson Research Center, 1101 Kitchawan Rd., Yorktown Heights, NY 10598, USA

Abstract. In this work, an accurate and suitable data reduction scheme is developed to measure the fracture energy of adhesive joints under pure mode I loading. The method is based on the crack equivalent concept and is applied to the Double Cantilever Beam specimen. Using the proposed methodology it is not necessary to measure the crack length during propagation, which can introduce non-negligible errors on the fracture energy measurements. Moreover, it accounts for the Fracture Process Zone effects which can be significant when ductile adhesives are used. The new method was compared to classical data reduction schemes and was validated numerically using a trapezoidal mixed-mode cohesive damage model. The fracture characterization in mode I using a developed trapezoidal cohesive damage model is performed by an inverse method. Excellent agreement between the numerical and experimental *R*-curves was achieved demonstrating the adequacy of the proposed method.

Keywords: A. Adhesive joints, B. Fracture toughness, C. Finite element analysis (FEA), Cohesive damage models

1. Introduction

Adhesively bonded joints are being increasingly used due to their interesting characteristics. Adhesive joints behave well under fatigue loads, allow joining different materials and present less stress concentrations than alternative joining techniques. In

order to increase the confidence of designers, it is essential to accurately predict their strength. In this context, fracture mechanics approaches present some important advantages over strength of materials based methods. In fact, the strength based methods do not provide a rigorous description of the structures' behaviour when stress singularities are present. Fracture mechanics approach is frequently applied by means of an energetic analysis. In fact, Kinloch [1] refers that the energetic criterion is advantageous relatively to the stress intensity factors approach. First, the strain energy release rate has an important physical significance related to the energy absorption. Second, the determination of the stress intensity factors is not easy, namely when the crack grows at or near an interface. In this context, the determination of the critical fracture energies of the bonded joints acquire special relevancy.

Several authors addressed the critical fracture energy determination of bonded joints under pure mode I. Recently, Cohesive Zone Models (CZM) have been used to simulate damage onset and growth in order to accurately predict the fracture behaviour of bonded joints. Blackman et al. [2] used a CZM approach on Tapered Double Cantilever Beam (TDCB) and peel tests under mode I load including two parameters, G_c and σ_{max}, to study the fracture of adhesively bonded joints. A polynomial traction-separation law was considered and special attention was dedicated to the physical significance of σ_{max}. It was concluded that the specimen's compliance and G_c depend on the value of σ_{max} until a relatively high value of this parameter, when the dependence significantly diminished. Andersson and Stigh [3] used an inverse method to determine the cohesive parameters of a ductile adhesive layer used in a Double Cantilever Beam (DCB) specimen. It was verified that the stress-relative displacement relationship can be divided in three parts. Initially the stress increases proportionally to the elongation (linear elastic behaviour of the adhesive layer), until a limit stress is achieved. A plateau

region is then observed, corresponding to the plastic behaviour of the adhesive. The curve ends with a parabolic softening part. A similar constitutive softening law was used by Tvergaard and Hutchinson [4, 5] and Yang et al. [6, 7].

The majority of joints fracture characterization under pure mode I is performed using the DCB specimen [3, 8-10]. The main advantages of this experimental test include its simplicity and the possibility to obtain the fracture toughness mathematically using the beam theory [11]. However, some issues must be taken into account to accurately measure the critical fracture energy. In fact, unstable crack propagation was experimentally verified by Bader et al. [8] and Ducept et al. [9], which hinders a clear crack length monitoring during the test. On other cases, in the DCB test of bonded joints, the crack tip may not be clearly visible depending on the adhesive. This can induce non negligible errors on the derivative of the compliance relatively to the crack length (dC/da) used in the Compliance Calibration Method (CCM). On the other hand, the energy dissipated at the Fracture process Zone (FPZ) can be large, namely when ductile adhesives are used [12]. This implies that beam theory based methods without any corrections underestimate the adhesive fracture energy.

The objective of this work is to provide a suitable methodology for fracture characterization of bonded joints under pure mode I loading. A new data reduction scheme based on the crack equivalent concept is presented and applied to the DCB test to obtain the respective critical fracture energy. The proposed model does not require crack length monitoring during propagation and accounts for the FPZ effects. Additionally, the influence of the Young´s modulus scattering between different specimens is also taken into account considering an equivalent elastic modulus. The model is compared with classical reduction schemes, such as the CCM, Direct Beam Theory (DBT) and Corrected Beam Theory (CBT). A numerical analysis including a

developed trapezoidal mixed-mode cohesive damage model adequate for ductile adhesives was also conducted to validate the new data reduction scheme. Some of the cohesive properties of the trapezoidal law were determined using an inverse method, allowing the complete fracture characterization of the adhesive under mode I loading.

2. Experimental work

The geometry of the DCB specimens is presented in Fig. 1 (L=120 mm, a_0=45 mm, 2h=5.2 mm, B=15 mm, t=0.2 mm). The adherends consist of unidirectional 0º lay-ups of carbon/epoxy prepreg (SEAL® Texipreg HS 160 RM) with 16 plies, whose lamina mechanical properties are presented in Table 1 [13]. Curing of the adherends was achieved in a press during one hour at 130ºC and 4 bar pressure. A ductile epoxy adhesive (Araldite® 2015) was used, whose elastic properties were measured experimentally in bulk tests (Young's modulus E=1850 MPa, Poisson's ratio ν=0.3). The bonding process included roughening, with sandpaper, the surfaces to be bonded and cleaning them with acetone to increase the adhesion and avoid adhesive failures, followed by adhesively bonding the laminates and curing at room temperature. A constant adhesive thickness (0.2 mm) was guaranteed by placing, during the curing process of the adhesive, calibrated steel bars (0.20±0.01 mm) between the adherends. The final adhesive thickness was measured in order to verify its correctness. Piano hinges were adhesively-bonded to the laminates, allowing the application of the load. The initial crack was introduced with a razor blade, using calibrated bars on both sides to guide it through the specimen, assuring its position in the adhesive mid-thickness. In order to avoid a blunt crack, all specimens were afterwards slightly loaded to ensure 1-2 mm of crack propagation, after which a_0 was measured in an optical microscope. Testing was then initiated. Five specimens were tested on a testing machine (Instron 4208) at room temperature. They were subjected to a tensile loading under displacement

control (2 mm/min). The load-displacement (P-δ) curve was registered during the test. Pictures were recorded during the specimens testing with 5 s intervals using a 10 MPixel digital camera. This procedure allows measuring the crack length during its growth and afterwards collecting the P-δ-a parameters. This was performed correlating the time elapsed since the beginning of each test between the P-δ curve and each picture (the testing time of each P-δ curve point is obtained accurately with the absolute displacement and the established loading rate). The picture in Fig. 2 was recorded during a test and shows the crack tip, allowing the crack length measurement. Cohesive fractures were obtained for all specimens.

3. Data reduction schemes

3.1 Classical methods

The classical reduction schemes to obtain the critical fracture energy in pure mode I (J_{Ic}) are usually based on compliance calibration or the beam theory. The CCM is based on the Irwin-Kies equation [14]

$$J_{Ic} = \frac{P^2}{2B}\frac{dC}{da} \tag{1}$$

where P represents the load, B the specimen width and $C=\delta/P$ the compliance. Cubic polynomials ($C=C_3a^3+C_2a^2+C_1a+C_0$) were used to fit the $C=f(a)$ curves, leading to

$$J_{Ic} = \frac{P^2}{2B}\left(3C_3a^2 + 2C_2a + C_1\right) \tag{2}$$

Beam theories were also used to measure J_{Ic}. The DBT, based on elementary beam theory, gives

$$J_{Ic} = \frac{12a^2P^2}{B^2h^3E_1} \tag{3}$$

h representing the height of each specimen arm and E_1 the Young's modulus of the adherends in the longitudinal direction. Using the CBT, J_{Ic} is obtained using [15]

$$J_{Ic} = \frac{3P\delta}{2B\left(a+|\Delta|\right)} \tag{4}$$

where Δ is a crack length correction for crack tip rotation and deflection. Using the beam theory, the relationship between the compliance and the crack length can be expressed as

$$C = \frac{8\left(a+|\Delta|\right)^3}{E_1 B h^3} \tag{5}$$

which gives

$$C^{1/3} = \frac{2}{h\left(E_1 B\right)^{1/3}}\left(a+|\Delta|\right) \tag{6}$$

allowing to obtain Δ from a linear regression of $C^{1/3}$ versus a data.

3.2 Compliance Based Beam Method

The previous methods (CCM and CBT) depend on accurate crack length measurements during propagation, which is not easy to perform. In fact, a FPZ develops ahead of the crack tip in consequence of multiple micro-cracks nucleation through the adhesive thickness and plastification. This phenomenon renders difficult the identification of the crack tip locus. On the other hand, when ductile adhesives are used, the energy dissipated in the FPZ is not negligible and should be considered in the selected data reduction scheme. The method described in this section takes into account these features. It is named Compliance Based Beam Method (CBBM) and is based on the crack equivalent concept, depending only on the specimen's compliance during the test. The strain energy of the specimen (Fig. 1) due to bending and including shear effects is

$$U = 2\left[\int_0^a \frac{M_f^2}{2E_1 I}dx + \int_0^a \int_{-h/2}^{h/2} \frac{\tau^2}{2G_{13}} B\, dz\, dx\right] \tag{7}$$

where M_f is the bending moment, I the second moment of area of each arm, E_1 and G_{13} the elastic properties of the carbon-epoxy composite and

$$\tau = \frac{3}{2}\frac{V}{Bh}\left(1 - \frac{z^2}{c^2}\right) \tag{8}$$

The parameters c and V are, respectively, half-thickness and the transverse load on each arm ($0 \le x \le a$). From the Castigliano theorem the displacement δ, can be written as

$$\delta = \frac{\partial U}{\partial P} = \frac{8Pa^3}{E_1 Bh^3} + \frac{12Pa}{5BhG_{13}} \tag{9}$$

This equation constitutes an approach based on the beam theory and allows defining the compliance $C=\delta/P$ of the specimen from the P-δ curve. However, the beam theory does not account for all phenomena influencing the P-δ curve. For example, in the early initial linear part of the P-δ curve, there are stress concentrations at the crack tip whose effects are not included in the beam theory. To include these effects, a corrected flexural modulus (E_f) is used instead of E_1. The flexural modulus of the specimen can be obtained from equation (9) using the measured initial compliance (C_0)

$$E_f = \left(C_0 - \frac{12\left(a_0 + |\Delta|\right)}{5BhG_{13}}\right)^{-1} \frac{8\left(a_0 + |\Delta|\right)^3}{Bh^3} \tag{10}$$

where Δ is the root rotation correction on the initial crack length (a_0), used in equation (4). This parameter was obtained numerically for each specimen fitting the initial compliance with the experiments for the real a_0. After, two specimens with different initial crack lengths were simulated, thus defining three points for the $C^{1/3}$=f(a) relation. On the other hand, an equivalent crack length (a_e) must be considered during propagation to account for the FPZ effects at the crack tip (Fig. 3). The equivalent crack

can be calculated from equation (9) as a function of the specimen compliance registered during the test and considering $a_e = a + |\Delta| + \Delta a_{FPZ}$ instead of a. The solution of the cubic equation can be obtained using the MATLAB® software. The fracture energy in mode I can now be obtained using equation (1), leading to

$$J_{Ic} = \frac{6P^2}{B^2 h}\left(\frac{2a_e^2}{h^2 E_f} + \frac{1}{5G_{13}}\right) \tag{11}$$

This method does not require monitoring the crack length during propagation. In fact, the crack length is calculated as a function of the specimen compliance during the test, which allows including the FPZ effects on the measured fracture energy.

4. Experimental results

The experimental P-δ curves of the DCB specimens are presented in Fig. 4. The critical fracture energy in mode I was evaluated using the four methods presented in section 3. Fig. 5 shows the experimental R-curves obtained by all methods for one tested specimen. Table 2 presents the results of all specimens. Similar results were obtained by CBT and CBBM. The CCM presents a slight difference, explained by polynomial fitting difficulties. The DBT method presents a smaller J_{Ic} for all tested specimens. In fact, this method does not include crack length corrections in order to account for root rotation and shear effects, which explains the underestimated results. It should be noted that the CBBM R-curve is out of phase to the right relatively to the remaining ones, since the equivalent crack used in this method is higher than the real crack length measured during the tests and used in the other methods (Fig. 5).

5. Numerical analysis

A trapezoidal mixed-mode cohesive damage model was developed to numerically simulate the adhesive behaviour in mode I. The model was implemented within

interface finite elements in the ABAQUS® software. An inverse method will be used to obtain the cohesive law in mode I. This model will be used to evaluate the adequacy of the data reduction schemes used to obtain J_{Ic}. The inputted J_{Ic} will be compared to the values provided by the different methods.

5.1. Trapezoidal cohesive damage model

A mixed-mode (I+II) cohesive damage model implemented within interface finite elements was developed to simulate damage onset and growth. The adhesive layer is simulated by these elements, which have zero thickness. To simulate the behaviour of ductile adhesives, a trapezoidal softening law relating stresses ($\boldsymbol{\sigma}$) and relative displacements ($\boldsymbol{\delta}_r$) between homologous points of the interface elements was employed (Fig. 6). These types of laws accurately reproduced the behaviour of thin ductile adhesive layers in mode I [3] and mode II [16]. The constitutive relationship before damage onset is

$$\boldsymbol{\sigma} = \mathbf{E}\boldsymbol{\delta}_r \tag{12}$$

where $\mathbf{E}$ is a stiffness diagonal matrix containing the stiffness parameters e_i (i=I, II) defined as the ratio between the elastic modulus of the material in tension or shear (E or G, respectively) and the adhesive thickness t. Considering the pure-mode model, after $\delta_{1,i}$ (the first inflexion point, which leads to the plateau region of the trapezoidal law) the material softens progressively or, in other words, undergoes damage. This is simulated by the energy being released in a cohesive zone ahead of the crack tip. This region, known as Fracture Process Zone, is where the material undergoes softening damage by different ways, e.g., microscopic cracks and extensive plasticity. Numerically, this is implemented using a damage parameter whose values vary from zero (undamaged) to unity (complete loss of stiffness) as the material deteriorates. The softening relationship can be written as

$$\boldsymbol{\sigma} = (\mathbf{I} - \mathbf{D})\mathbf{E}\boldsymbol{\delta}_{\mathbf{r}} \tag{13}$$

where **I** is the identity matrix and **D** is a diagonal matrix containing, on the position corresponding to mode i (i=I, II) the damage parameter. In the plateau region the damage parameter can be defined as

$$d_i = 1 - \frac{\delta_{1,i}}{\delta_i} \tag{14}$$

and, in the stress softening part of the curve

$$d_i = 1 - \frac{\delta_{1,i}\left(\delta_{\mathrm{u},i} - \delta_i\right)}{\delta_i\left(\delta_{\mathrm{u},i} - \delta_{2,i}\right)} \tag{15}$$

where δ_i is the current relative displacement and $\delta_{2,i}$ is the second inflexion point of the trapezoidal law, both in each mode (i=I, II). The maximum relative displacement, $\delta_{\mathrm{u},i}$, at which complete failure occurs, is obtained by equating the area under the softening curve to $J_{i\mathrm{c}}$, which corresponds to the respective critical fracture energy

$$J_{ic} = \frac{\sigma_{\mathrm{u},i}}{2}\left(\delta_{2,i} - \delta_{1,i} + \delta_{\mathrm{u},i}\right) \tag{16}$$

where $\sigma_{\mathrm{u},i}$ represents the local strength in each mode (i=I, II). In general, bonded joints are under mixed-mode loading. Therefore, a formulation for interface finite elements should include a mixed-mode damage model, which is an extension of the described pure-mode model (Fig. 6). Damage onset is predicted using a quadratic stress criterion

$$\begin{aligned} &\left(\frac{\sigma_{\mathrm{I}}}{\sigma_{\mathrm{u,I}}}\right)^2 + \left(\frac{\sigma_{\mathrm{II}}}{\sigma_{\mathrm{u,II}}}\right)^2 = 1 \quad \text{if} \quad \sigma_{\mathrm{I}} > 0 \\ &\sigma_{\mathrm{II}} = \sigma_{\mathrm{u,II}} \qquad\qquad\qquad\quad \text{if} \quad \sigma_{\mathrm{I}} \le 0 \end{aligned} \tag{17}$$

where σ_i, (i=I, II) represent the stresses in each mode. It is assumed that normal compressive stresses do not induce damage. Considering equation (12), the first equation (17) can be rewritten as a function of the relative displacements

$$\left(\frac{\delta_{1\mathrm{m,I}}}{\delta_{1,\mathrm{I}}}\right)^2+\left(\frac{\delta_{1\mathrm{m,II}}}{\delta_{1,\mathrm{II}}}\right)^2=1 \tag{18}$$

where $\delta_{1\mathrm{m},i}$ (i=I, II) are the relative displacements in each mode corresponding to damage initiation. Defining an equivalent mixed-mode displacement

$$\delta_{\mathrm{m}}=\sqrt{\delta_{\mathrm{I}}^{2}+\delta_{\mathrm{II}}^{2}} \tag{19}$$

and mixed-mode ratio (i=I, II)

$$\beta_i=\frac{\delta_i}{\delta_{\mathrm{I}}} \tag{20}$$

the mixed-mode relative displacement at the onset of the softening process ($\delta_{1\mathrm{m}}$) can be obtained combining equations (18), (19) and (20)

$$\delta_{1\mathrm{m}}=\delta_{1,\mathrm{I}}\delta_{1,\mathrm{II}}\sqrt{\frac{1+\beta_{\mathrm{II}}^{2}}{\delta_{1,\mathrm{II}}^{2}+\beta_{\mathrm{II}}^{2}\delta_{1,\mathrm{I}}^{2}}} \tag{21}$$

Stress softening onset ($\delta_{2,i}$) was predicted using a quadratic relative displacements criterion similar to (18), leading to

$$\left(\frac{\delta_{2\mathrm{m,I}}}{\delta_{2,\mathrm{I}}}\right)^2+\left(\frac{\delta_{2\mathrm{m,II}}}{\delta_{2,\mathrm{II}}}\right)^2=1 \tag{22}$$

where $\delta_{2\mathrm{m},i}$ (i=I, II) are the relative displacements in each mode corresponding to stress softening onset. Using a procedure similar to the one followed for $\delta_{1\mathrm{m}}$, the mixed-mode relative displacement at the onset of the stress softening process ($\delta_{2\mathrm{m}}$) can be obtained

$$\delta_{2\mathrm{m}}=\delta_{2,\mathrm{I}}\delta_{2,\mathrm{II}}\sqrt{\frac{1+\beta_{\mathrm{II}}^{2}}{\delta_{2,\mathrm{II}}^{2}+\beta_{\mathrm{II}}^{2}\delta_{2,\mathrm{I}}^{2}}} \tag{23}$$

Crack growth was simulated by the linear fracture energetic criterion

$$\frac{J_{\mathrm{I}}}{J_{\mathrm{Ic}}}+\frac{J_{\mathrm{II}}}{J_{\mathrm{IIc}}}=1 \tag{24}$$

When equation (24) is satisfied damage growth occurs and stresses are released, with the exception of normal compressive ones. The energy released in each mode at complete failure (J_i, i=I, II) is obtained from the area of the smaller trapezoid of Fig. 6

$$J_i = \frac{\sigma_{\mathrm{um},i}}{2}\left(\delta_{2\mathrm{m},i} - \delta_{1\mathrm{m},i} + \delta_{\mathrm{um},i}\right) \tag{25}$$

Combining equations (16), (25) and (24) the ultimate mixed-mode relative displacement (δ_{um}) can be written as

$$\delta_{\mathrm{um}} = \frac{2J_{\mathrm{Ic}}J_{\mathrm{IIc}}\left(1+\beta_{\mathrm{II}}{}^2\right) - \delta_{1\mathrm{m}}\left(\delta_{2\mathrm{m}} - \delta_{1\mathrm{m}}\right)\left(e_{\mathrm{I}}J_{\mathrm{IIc}} + \beta_{\mathrm{II}}{}^2 e_{\mathrm{II}}J_{\mathrm{Ic}}\right)}{\delta_{1\mathrm{m}}\left(e_{\mathrm{I}}J_{\mathrm{IIc}} + \beta_{\mathrm{II}}{}^2 e_{\mathrm{II}}J_{\mathrm{Ic}}\right)} \tag{26}$$

The equivalent quantities $\delta_{1\mathrm{m}}$, $\delta_{2\mathrm{m}}$ and δ_{um} are then used in equations (14) and (15) in order to define the damage parameter.

5.2. Evaluation of the cohesive parameters

The profile of the cohesive law was chosen due to the known typical behaviour of the ductile adhesive used which, after an initial linear σ-ε relationship, presents a plateau corresponding to plastic behaviour. Consequently, the inflexion points have a physical significance. However, it is known that bulk adhesives behave differently as thin layer adhesives due to constraint effects induced by the adherends. As a result, bulk properties should not be used and the trapezoidal cohesive law parameters should be determined by an inverse method, as described below.

Initially, the experimental load-displacement curve is used to obtain the respective *R*-curve using the CBBM. The fracture energy, which corresponds to the plateau value of the *R*-curve, is considered as an inputted parameter in the numerical approach, which includes the trapezoidal mixed-mode cohesive damage model in order to simulate damage initiation and growth. In the following step, some numerical iterations should

be performed until a good accuracy between the numerical and experimental P-δ curves is obtained (Fig. 7), thus defining the remaining cohesive parameters ($\sigma_{u,I}$ and $\delta_{2,I}$).

The deformed shape of the DCB specimen during damage propagation and the applied boundary conditions are presented in Fig. 8. The specimen arms were modelled with plane strain 8-node quadrilateral solid finite elements (CPE8 from the ABAQUS® library) and the adhesive was modelled with 6 node interface elements, including the trapezoidal mixed-mode cohesive damage model. Five solid finite elements were used through-thickness in each arm, with a more refined mesh near the adhesive region and the respective outer surface. In the damage propagation region a more refined mesh was used (Fig. 8), considering 0.15 mm length elements. Boundary conditions included clamping the lower edge node of the lower arm, applying a vertical displacement and horizontally restraining the upper edge node of the upper arm (Fig. 8).

It was verified that $\sigma_{u,I}$ does not greatly influence the P-δ curve (Fig. 9). Consequently, $\sigma_{u,I}$ was fixed at 23 MPa, which is the average value over all specimens. The influence of $\delta_{2,I}$ on the P-δ curve was also assessed. R represents the ratio between the ascending and descending parts of the trapezoidal law displacements, given by (Fig. 6)

$$R = \frac{\delta_{u,I} - \delta_{2,I}}{\delta_{1,I}} \tag{27}$$

It was verified that this parameter practically does not influence the P-δ curve profile for $0.5 \leq R \leq 2$ and R=1 was used in the simulations. Fig. 10 shows the average J_{Ic}, $\delta_{2,I}$ and $\delta_{u,I}$ and the trapezoidal laws range obtained fitting the five experimental P-δ curves.

6. Comparison between the numerical and experimental results

In order to verify the adequacy of the data reduction schemes used to measure accurately J_{Ic}, numerical simulations of the DCB tests were performed. The objective is to verify how the used methods reproduce the inputted J_{Ic}. The numerical P-δ-a

parameters were collected to obtain the respective *R*-curves. Fig. 11 shows the results for one case. The CBBM and CBT provide the most accurate results, when compared to the inputted value. However, it should be noted that the CBT requires the crack length monitoring during propagation, which is not easy to perform experimentally and is prone to introduce additional errors. On the other hand, the CBBM provides a complete *R*-curve and accounts for the energy dissipation at the FPZ. Fig. 12 also demonstrates the good performance of CBBM, when compared with the respective experimental *R*-curve, for the same specimen used in Fig. 7. Table 3 presents the global results of J_{Ic} predicted by the several methods, the respective error relatively to the inputted value and the average error based on absolute error values for each method. The CBBM yields the best results, with an average error of 0.5%. The CBT also agrees with the inputted J_{Ic} for all specimens. An error of 5.6% was obtained using the CCM, due to polynomial fitting difficulties. The bigger discrepancies are obtained with the DBT, which results in J_{Ic} values 14.9% lower than the inputted ones.

7. Conclusions

In this work a suitable methodology for fracture characterization under pure mode I of ductile adhesives used in bonded joints is performed. A new data reduction scheme based on crack equivalent concept is used to obtain J_{Ic} considering the DCB specimen. The method is advantageous relatively to classical ones since it does not require crack length measurement during its growth and accounts for the energy dissipated at the FPZ, which can be non negligible when ductile adhesives are used. When compared to classical data reduction schemes the method provided accurate results.

A numerical analysis was also performed to verify the adequacy of the several studied methods on the measurement of critical fracture energy under pure mode I loading. A trapezoidal mixed-mode cohesive damage model was developed to simulate the

behaviour of ductile adhesives. An inverse method was used to define the cohesive parameters of the trapezoidal law. The comparison between numerical and experimental results showed that the proposed CBBM provides accurate results on the critical fracture energy under pure mode I loading. Due to its advantages it can be considered the best choice for the fracture characterization of bonded joints.

Acknowledgements: The first author thanks the Portuguese Foundation for Science and Technology (PFST) for supporting the work here presented, through the research project POCI/EME/56567/2004. The second author thanks the PFST for supporting the work here presented through the individual grant SFRH/BD/30305/2006.

References

1. Kinloch AJ. Adhesion and adhesives: science and technology. Chapman & Hall, London, 1987.
2. Blackman BRK, Hadavinia H, Kinloch AJ, Williams JG. The use of a cohesive zone model to study the fracture of fibre composites and adhesively-bonded joints. Int J Fracture 2003;119:25–46.
3. Andersson T, Stigh U. The stress-elongation relation for an adhesive layer loaded in peel using equilibrium of energetic forces. Int J Solids Struct 2004;41:413-434.
4. Tvergaard V, Hutchinson JW. The influence of plasticity on the mixed-mode interface toughness. J Mech Phys Solids 993;41:1119–1135.
5. Tvergaard V, Hutchinson JW. On the toughness of ductile adhesive joints. J Mech Phys Solids 1996;44:789–800.
6. Yang QD, Thouless MD, Ward SM. Numerical simulations of adhesively-bonded beams failing with extensive plastic deformation. J Mech Phys Solids 1999;47:1337-1353.

7. Yang QD, Thouless MD, Ward SM. Elastic–plastic mode-II fracture of adhesive joints. Int J Solids Struct 2001;38:3251-3262.
8. Bader MG, Hamerton I, Hay JN, Kemp M, Winchester S. Double cantilever beam testing of repaired carbon fibre composites. Compos Part A 2000;31:603–608.
9. Ducept F, Davies P, Gamby D. Mixed mode failure criteria for a glass/epoxy composite and an adhesively bonded composite/composite joint. Int J Adhes Adhes 2000;20:233-244.
10. Nairn JA. Energy release rate analysis for adhesive and laminate double cantilever beam specimens emphasizing the effect of residual stresses. Int J Adhes Adhes 20;59-70:2000.
11. Yoshihara H. Simple estimation of critical stress intensity factors of wood by tests with double cantilever beam and three-point end-notched flexure. Holzforschung 2007;61:182–189.
12. de Moura MFSF. Numerical simulation of the ENF test for the mode-II fracture characterization of bonded joints. J Adhes Sci Technol 2006;20, 182-189.
13. Campilho RDSG, de Moura MFSF, Domingues JJMS. Modelling single and double-lap repairs on composite materials. Compos Sci Tech 2005;65:1948-1958.
14. Kanninen MF, Popelar CH. Advanced Fracture Mechanics. Oxford University Press, 1985.
15. de Moura MFSF, Pereira AB, de Morais AB. Influence of intralaminar cracking on the apparent interlaminar mode I fracture toughness of cross-ply laminates. Fatigue Fract Eng M 2004;27:759–766.
16. Leffler K, Alfredsson KS, Stigh U. Shear behaviour of adhesive layers. Int J Solids Struct 2007;44:530-545.

Figures

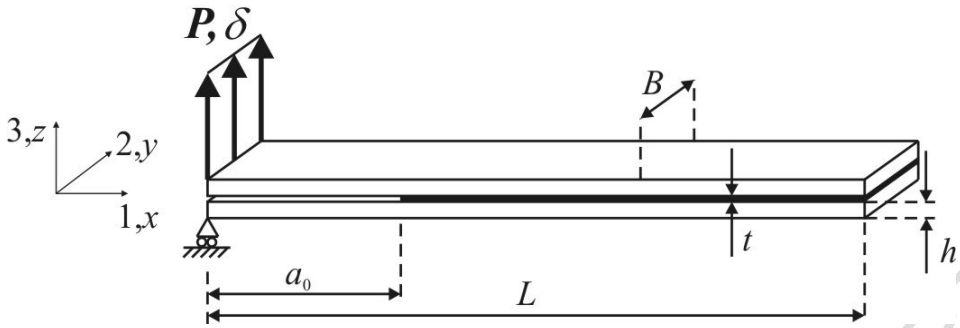

Fig. 1 – Schematic representation of the DCB test.

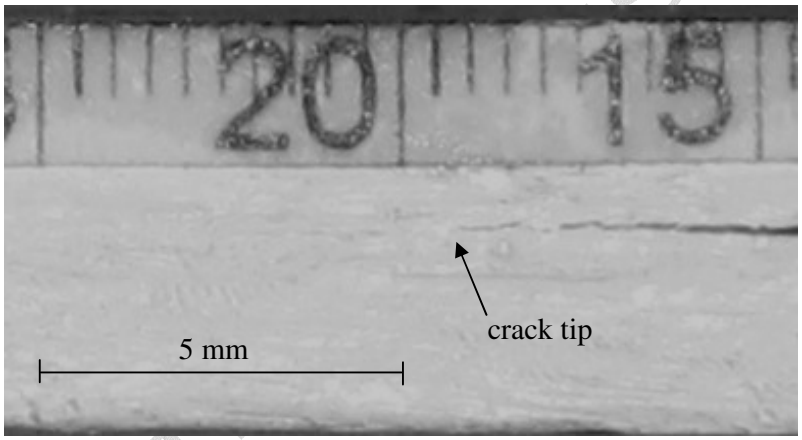

Fig. 2 – Experimental crack length measurement during propagation.

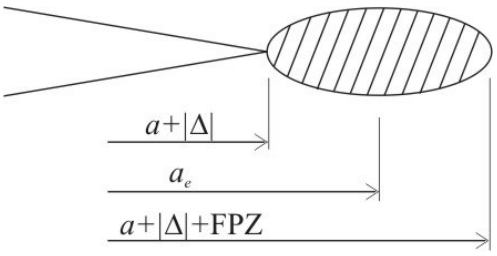

Fig. 3 – Schematic representation of the FPZ and crack equivalent concept.

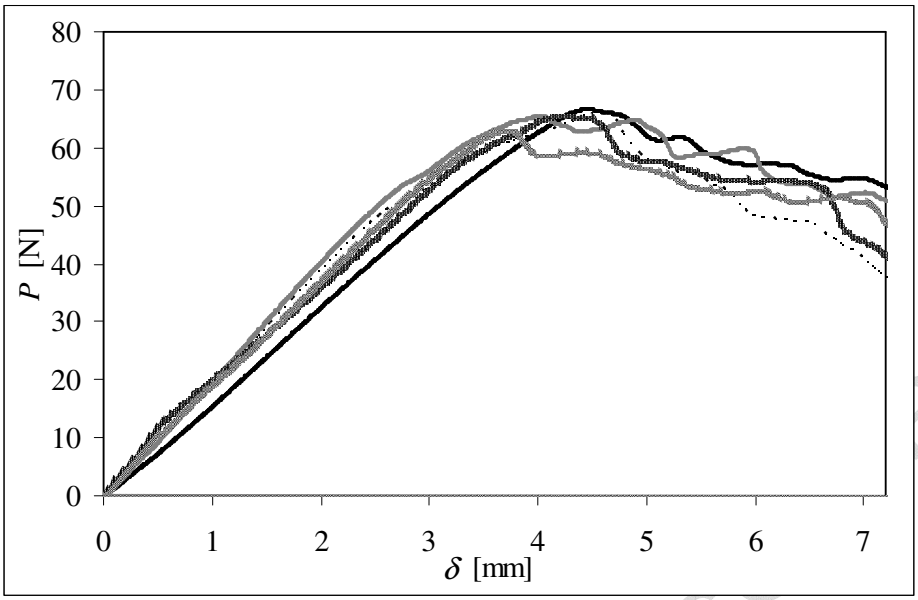

Fig. 4 – Experimental P-δ curves of the DCB specimens.

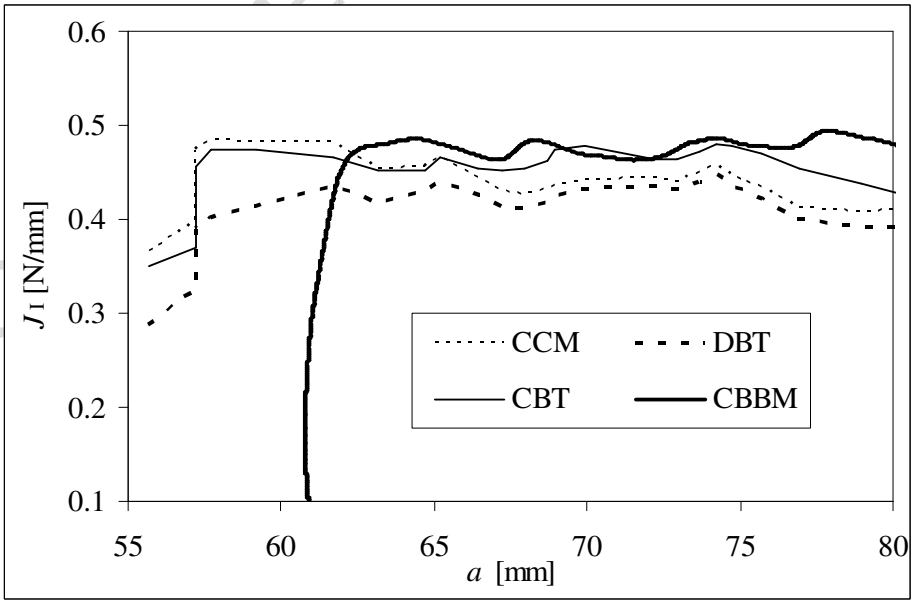

Fig. 5 – Experimental R-curves obtained by the different methods.

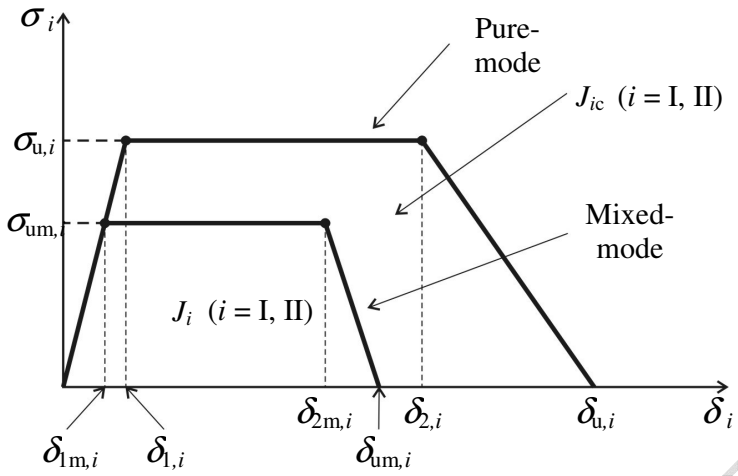

Fig. 6 – The trapezoidal softening law for pure-mode and mixed-mode.

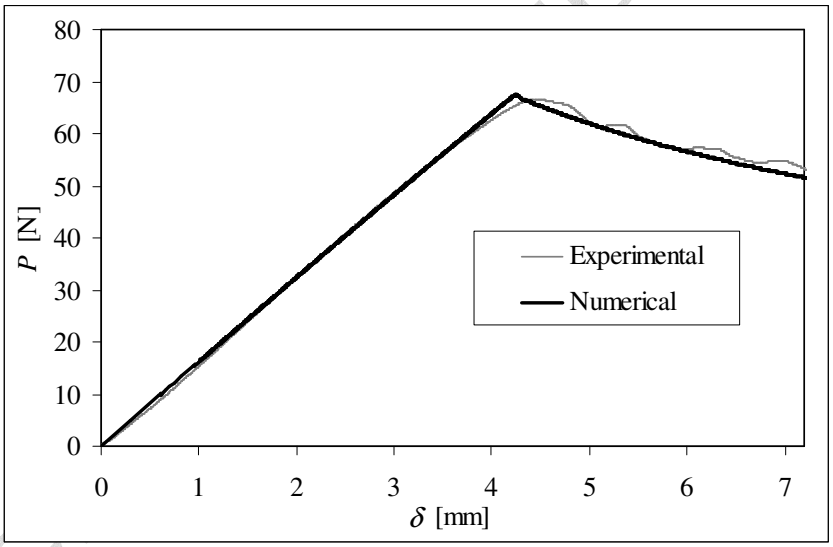

Fig. 7 – Comparison between numerical and experimental P-δ curves.

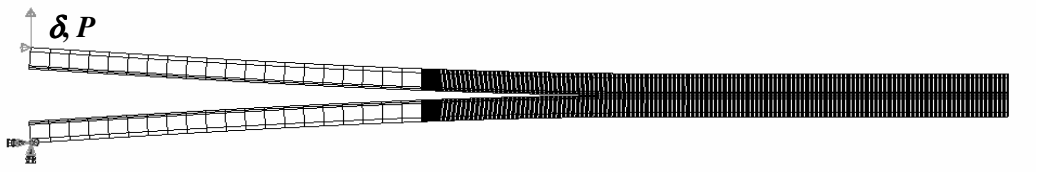

Fig. 8 –Deformed shape of the DCB specimen during propagation and boundary conditions.

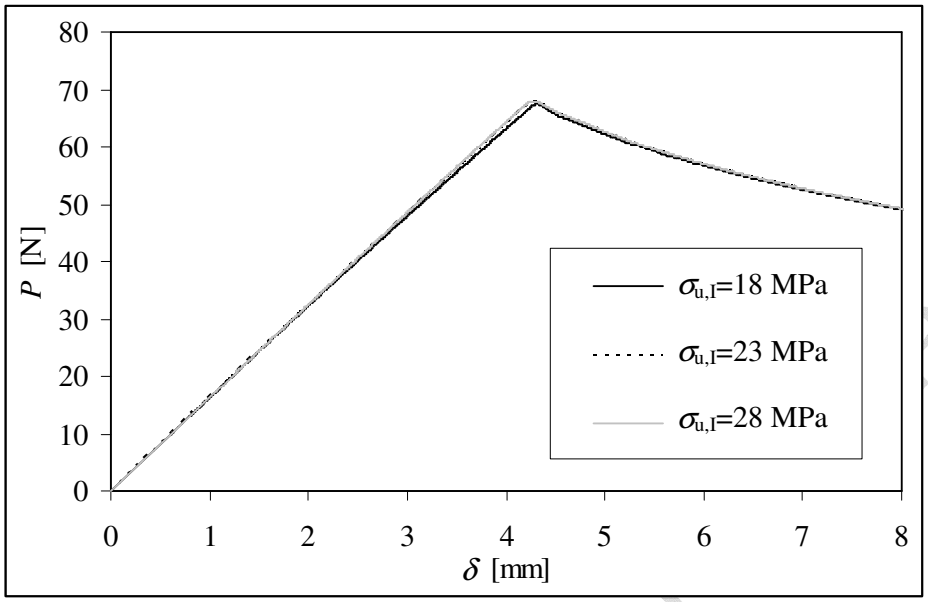

Fig. 9 – Influence of $\sigma_{u,I}$ on the P-δ curve.

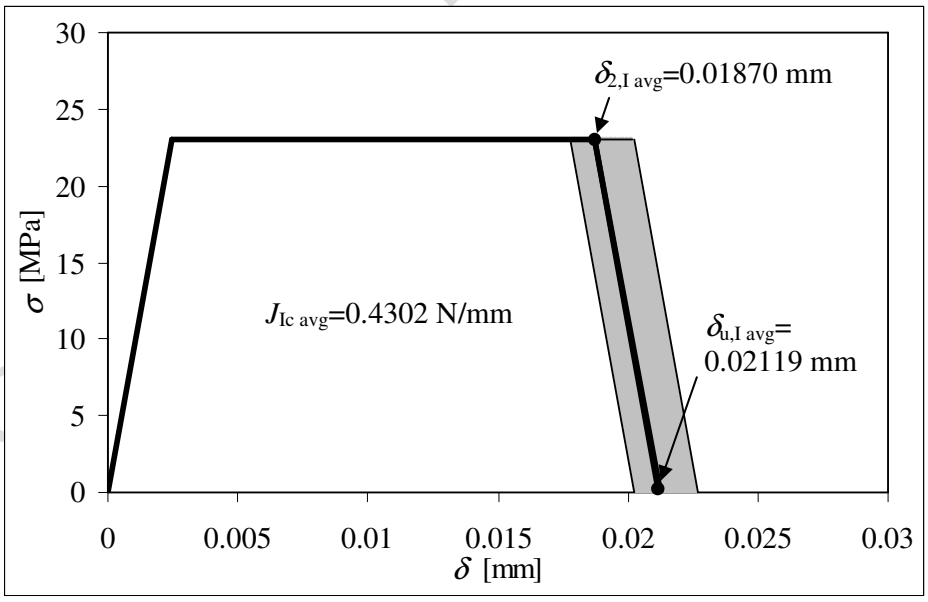

Fig. 10 – Trapezoidal cohesive laws range obtained with the five specimens and respective average values.

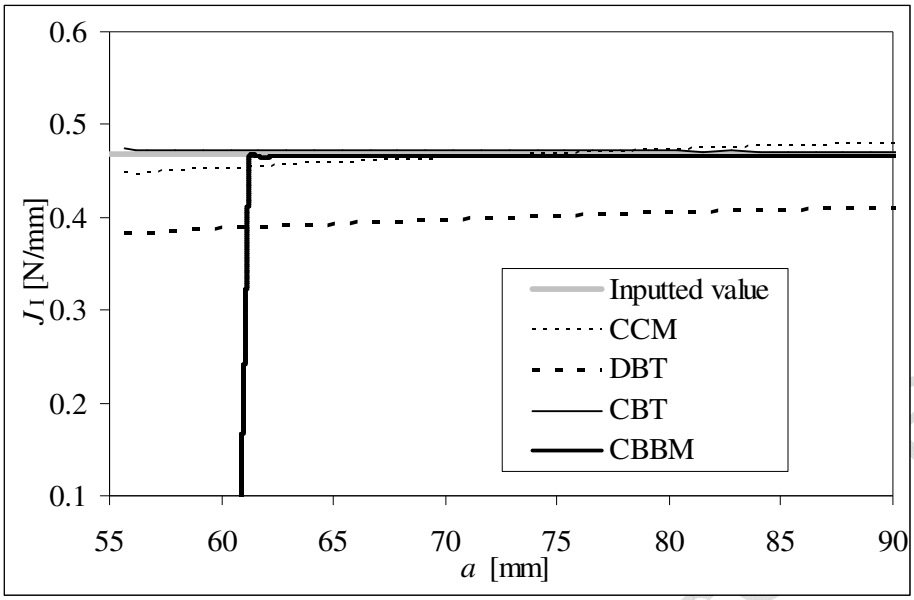

Fig. 11 – Numerical *R*-curves obtained by the different methods.

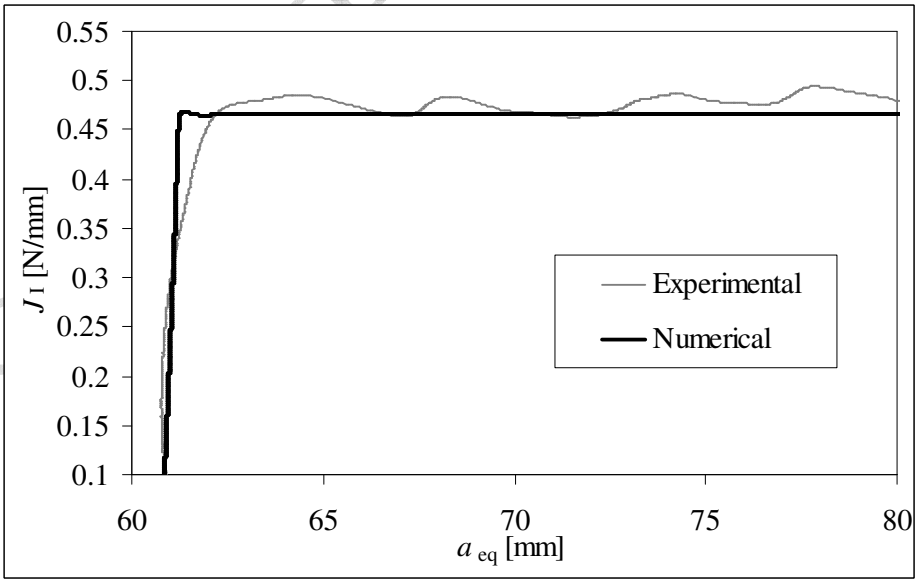

Fig. 12 – Comparison between numerical (CBBM) and experimental R-curves.

Tables

Table 1 – Carbon-epoxy lamina elastic properties.

E_1=1.09E+05 MPa	ν_{12}=0.342	G_{12}=4315 MPa
E_2=8819 MPa	ν_{13}=0.342	G_{13}=4315 MPa
E_3=8819 MPa	ν_{23}=0.380	G_{23}=3200 MPa

Table 2 – J_{Ic} (N/mm) values of the five specimens obtained by the different methods.

	CCM	DBT	CBT	CBBM
1	0.40	0.37	0.45	0.44
2	0.39	0.36	0.42	0.42
3	0.43	0.29	0.44	0.40
4	0.33	0.36	0.40	0.41
5	0.46	0.42	0.45	0.46
Avg. J_{Ic}	0.40	0.36	0.43	0.43
St. Dev.	0.04	0.04	0.02	0.02

Table 3 – Inputted and predicted J_{Ic} (N/mm) values by the several methods.

Spec.	Inp.	CCM	Err. [%]	DBT	Err. [%]	CBT	Err. [%]	CBBM	Err. [%]
1	0.444	0.420	-5.4	0.375	-15.5	0.448	1.0	0.442	-0.5
2	0.420	0.442	5.3	0.355	-15.6	0.422	0.5	0.416	-0.9
3	0.415	0.452	9.0	0.352	-15.1	0.423	2.0	0.413	-0.5
4	0.406	0.373	-8.2	0.348	-14.3	0.410	0.9	0.405	-0.3
5	0.468	0.469	0.2	0.402	-14.1	0.472	0.8	0.466	-0.3
Avg. Error [%]		5.6		14.9		1.0		0.5	